Supplementary information

Charge transport regulation in $Cu_{1.94}S$-ZnS-Co_9S_8 heterostructures via alignment engineering for photocatalytic hydrogen evolution

Weihuang Lin,[a] Ying Yang*,[a] Zhaozhe Chen,[b] Si Xiao,[b] and Weijia Wang*[c]

a. School of Metallurgy and Environment, Central South University, Changsha 410083, China. E-mail: **muyicaoyang@csu.edu.cn**.

b. School of Physics and Electronics, Central South University, Changsha, 410083, China.

c. Institute of Clinical Medicine, the Second Affiliated Hospital of Hainan Medical University, Haikou 570311, China. E-mail: **wangweijia@hainmc.edu.cn**

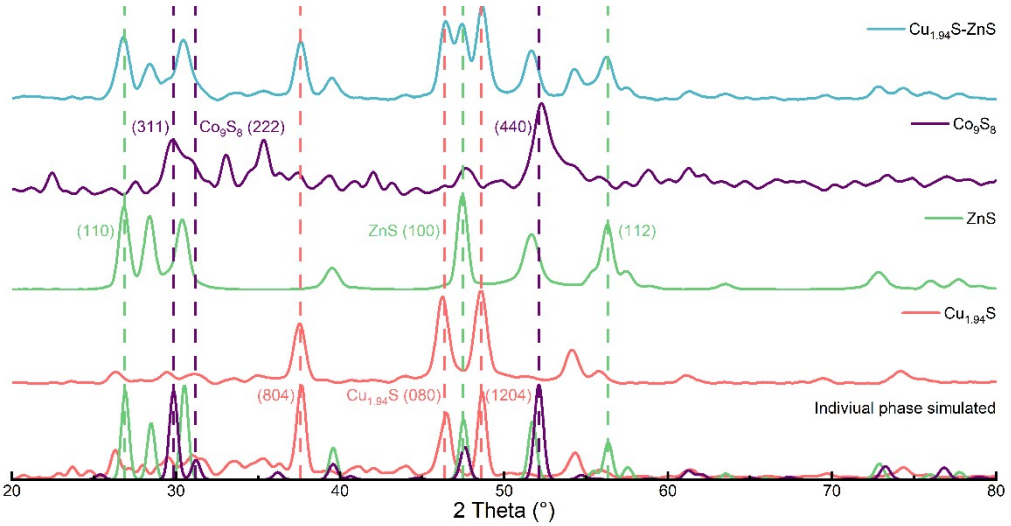

Fig. S1. Crystallographic analyses: Powder XRD patterns of $Cu_{1.94}S$-ZnS, Co_9S_8, ZnS, $Cu_{1.94}S$ nanocrystals and individual phase simulated diffraction profiles.

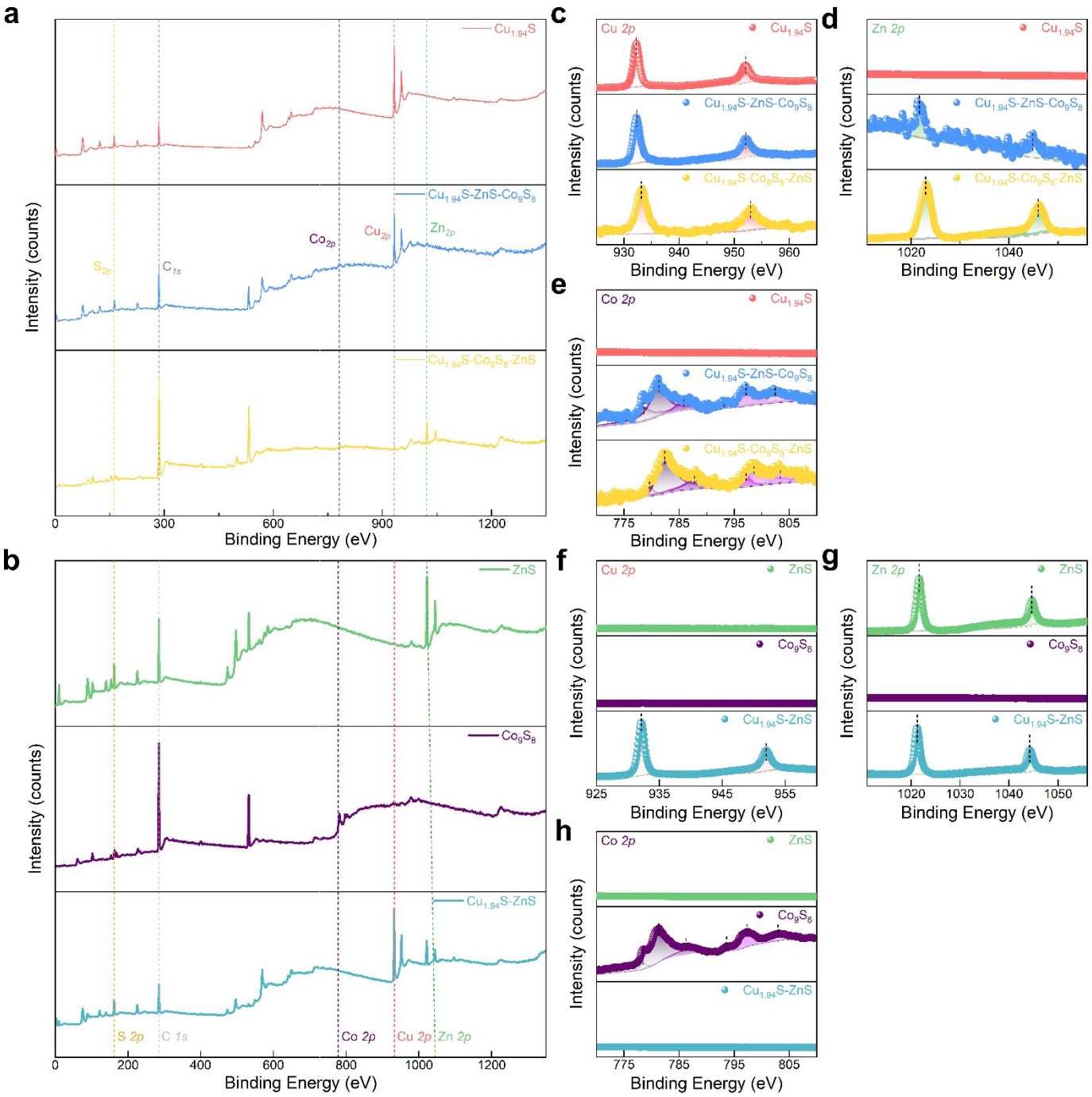

Fig. S2. Valence state analysis all nano particles: Full-spectrum XPS of all nanocrystals: (a & b) and high-resolution XPS spectra of Cu *2p* (c & f), Zn *2p* (d & g), and Co *2p* (e & h) for $Cu_{1.94}S$, $Cu_{1.94}S$-ZnS-Co_9S_8, $Cu_{1.94}S$-Co_9S_8-ZnS, ZnS, Co_9S_8 and $Cu_{1.94}S$-ZnS.

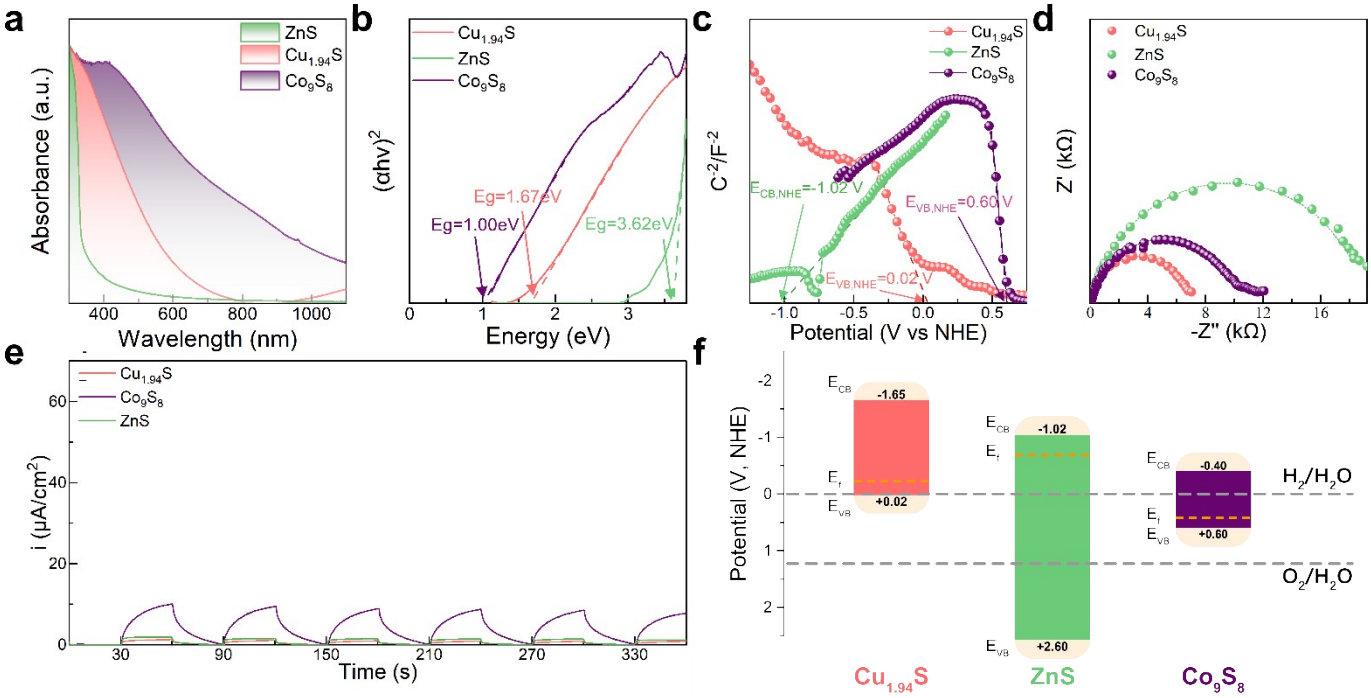

Fig. S3. Optical and electrochemical characterisations of the as-prepared samples: (a) Ultraviolet-visible-near infrared (UV-vis-NIR) absorption spectra and (b) corresponding Tauc plots of pristine $Cu_{1.94}S$, ZnS, and Co_9S_8. (c) Mott-Schottky plots and extracted flat-band potentials (V_{fb}) of the as-prepared samples. (d) Electrochemical impedance spectroscopy (EIS) Nyquist plots recorded under dark conditions. (e) Transient photocurrent density response of pristine individual components and (g) as-prepared binary/ternary NHs under chopped simulated solar irradiation. (f) Band alignment diagram derived from (b) and (c).

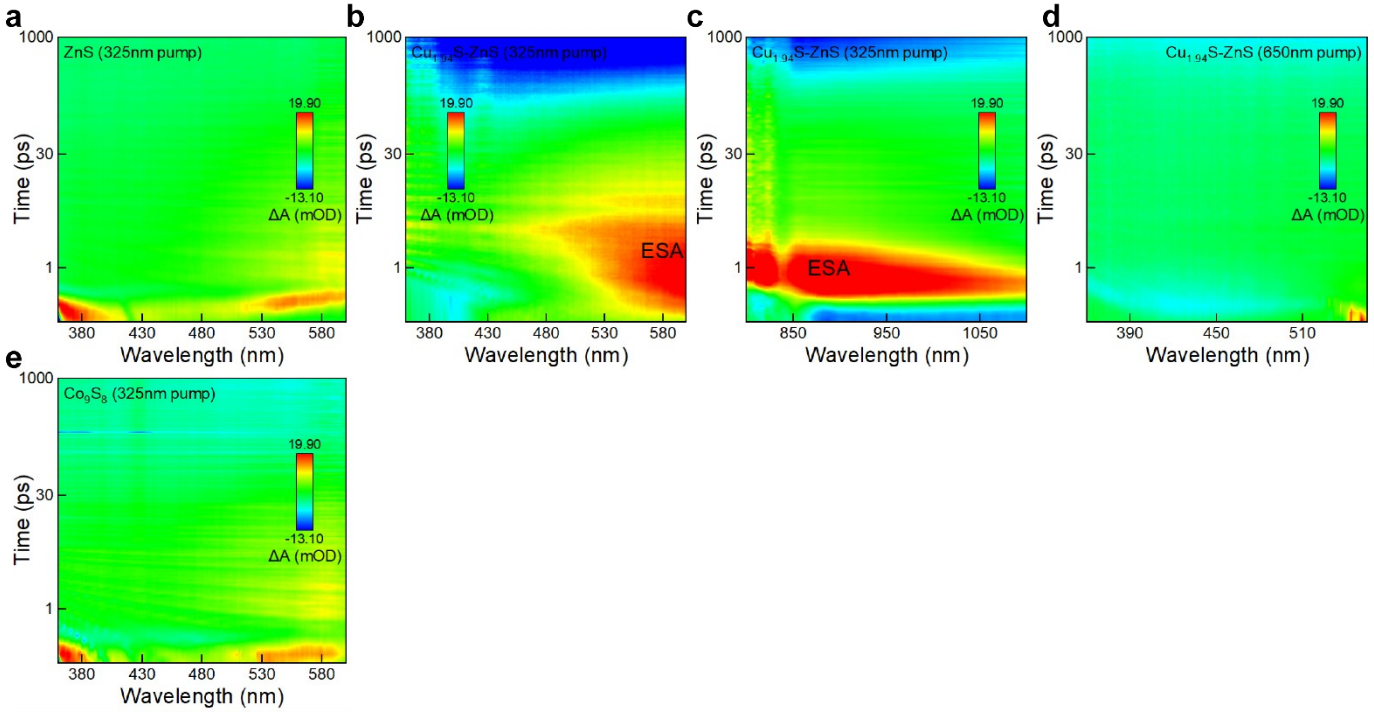

Fig. S4. Femtosecond transient absorption spectra of ZnS, $Cu_{1.94}S$-ZnS and Co_9S_8 (pump wavelength at 325/650 nm and probe at UV/NIR) with 2D pseudo color mapping for: (a) ZnS@325 nm pump and UV probe, (b) $Cu_{1.94}S$-ZnS@325 nm pump and UV probe, (c) $Cu_{1.94}S$-ZnS@325 nm pump and NIR probe, (d) $Cu_{1.94}S$-ZnS@650 nm pump and UV probe (e) Co_9S_8@325 nm pump and UV probe.

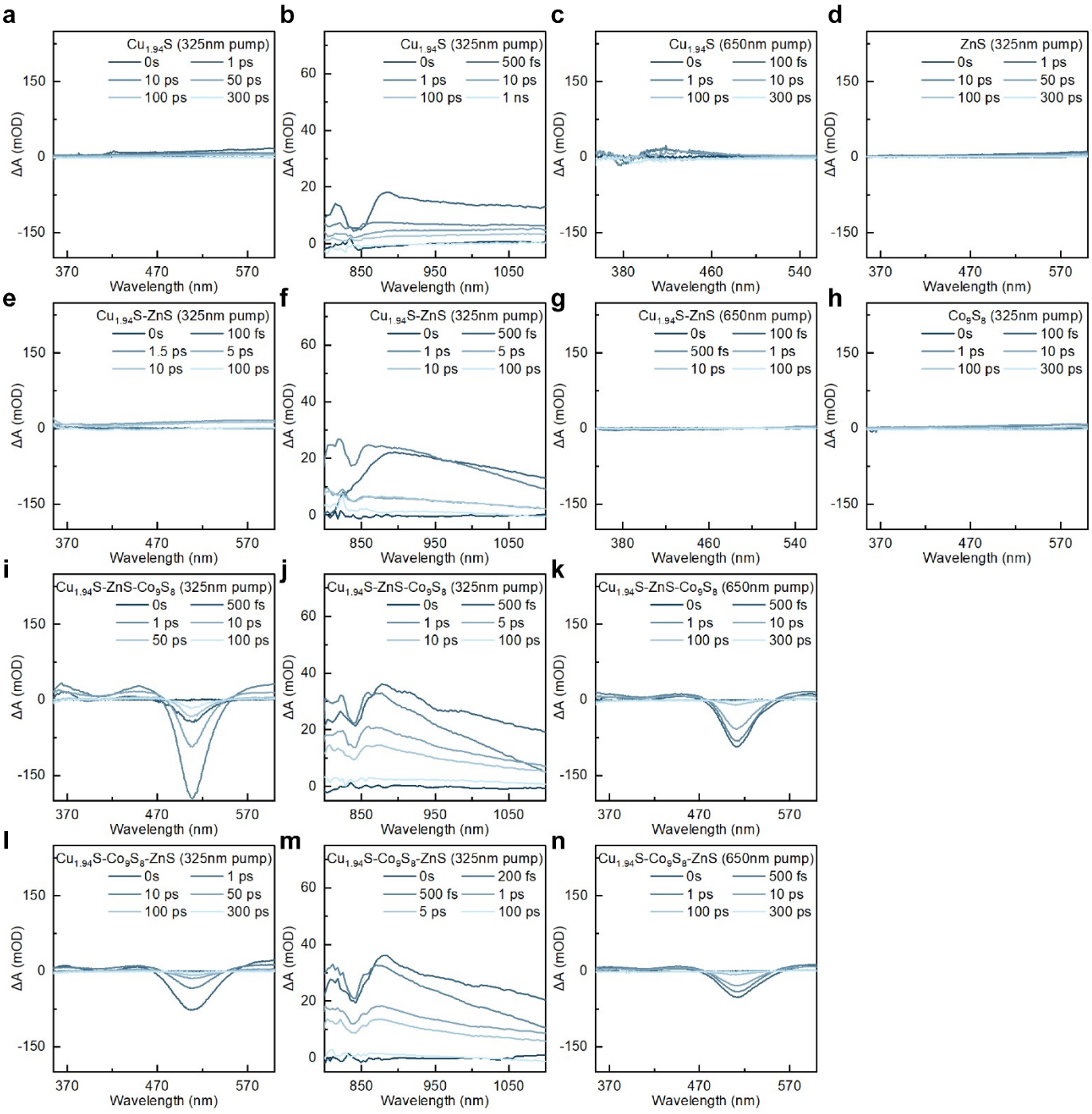

Fig. S5. Femtosecond transient absorption spectra of all nanocrystals at 325/650 nm and UV/NIR probe for: (a ~ c) $Cu_{1.94}S$, (d) ZnS, (e ~ g) $Cu_{1.94}S$-ZnS, (h) Co_9S_8, (I ~k) $Cu_{1.94}S$-ZnS-Co_9S_8 and $Cu_{1.94}S$-Co_9S_8-ZnS.

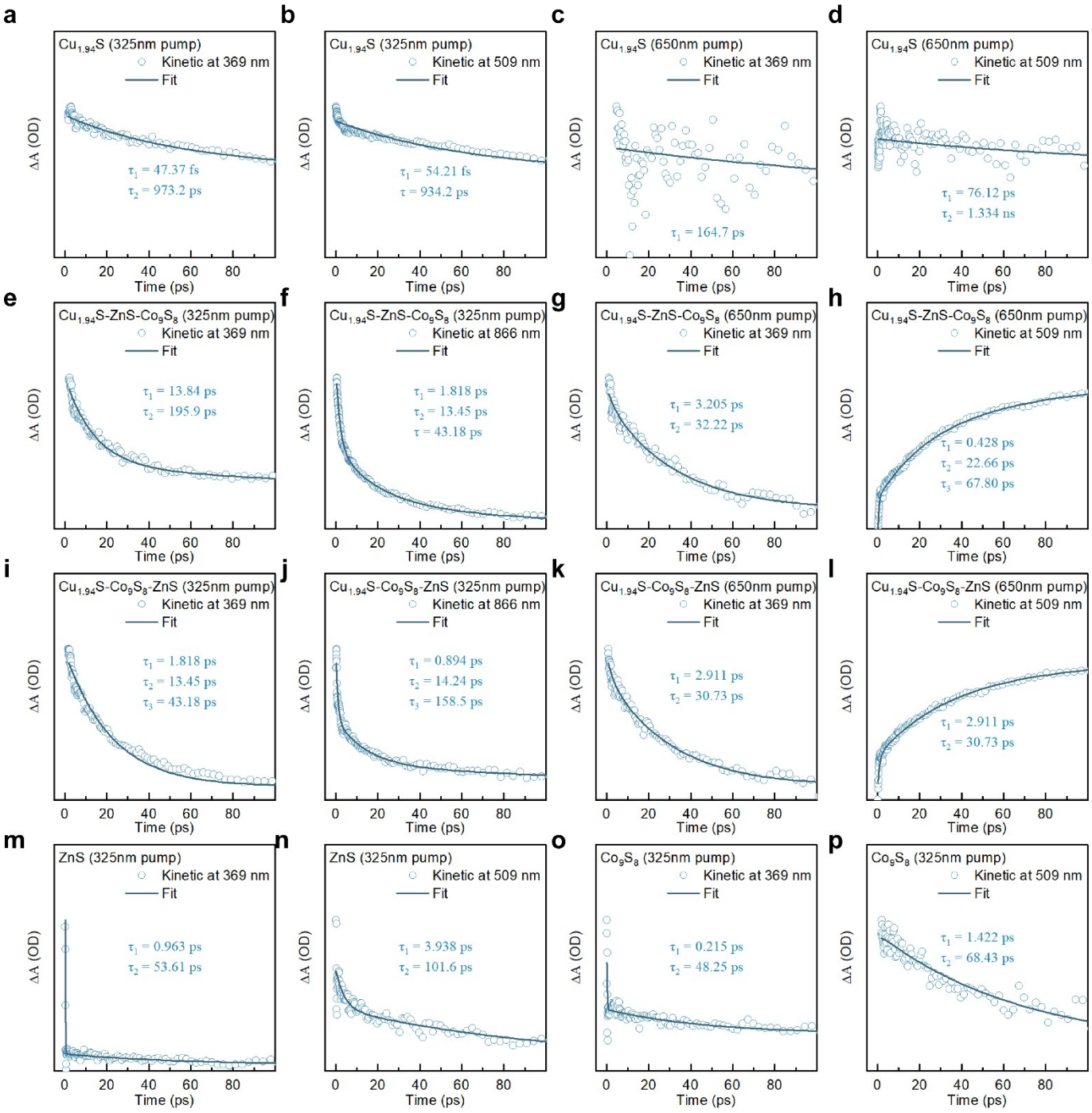

Fig. S6. Femtosecond transient absorption spectra of kinetic profiles (probing wavelength of 369, 509 and 866 nm) (pump wavelength: 325/650 nm) for: (a ~ d) $Cu_{1.94}S$, (e ~ h) $Cu_{1.94}S$-ZnS-Co_9S_8, (I ~ l) $Cu_{1.94}S$-Co_9S_8-ZnS, (m ~ n) ZnS and (o ~ p) Co_9S_8 nanocrystals.

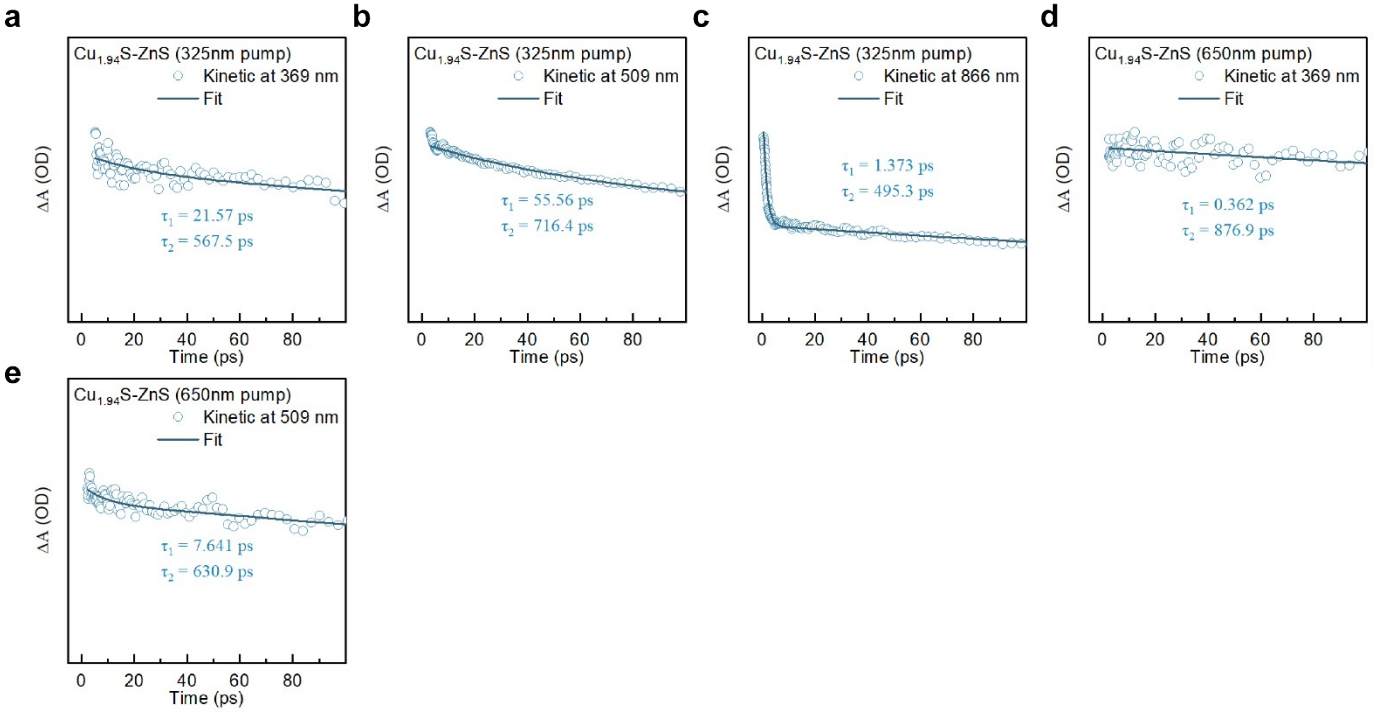

Fig. S7. Femtosecond transient absorption spectra of kinetic profiles (probing wavelength of 369, 509 and 866 nm) (pump wavelength: 325/650 nm) for: (a ~ e) $Cu_{1.94}S$-ZnS.

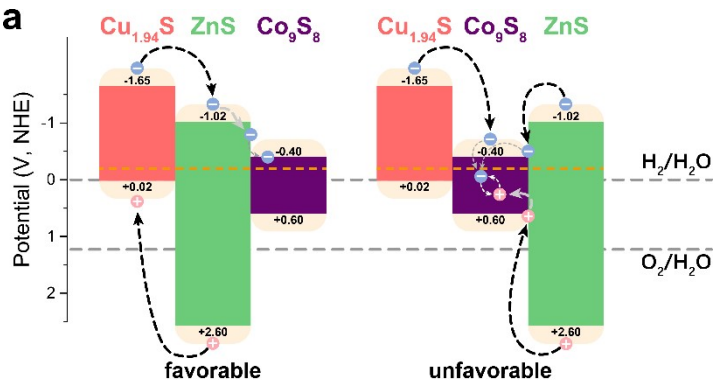

Fig. S8. Band structure and charge carrier dynamics analysis: (a) Schematic illustration of the band structures of $Cu_{1.94}S$-ZnS-Co_9S_8, $Cu_{1.94}S$-Co_9S_8-ZnS and interfacial charge transfer.

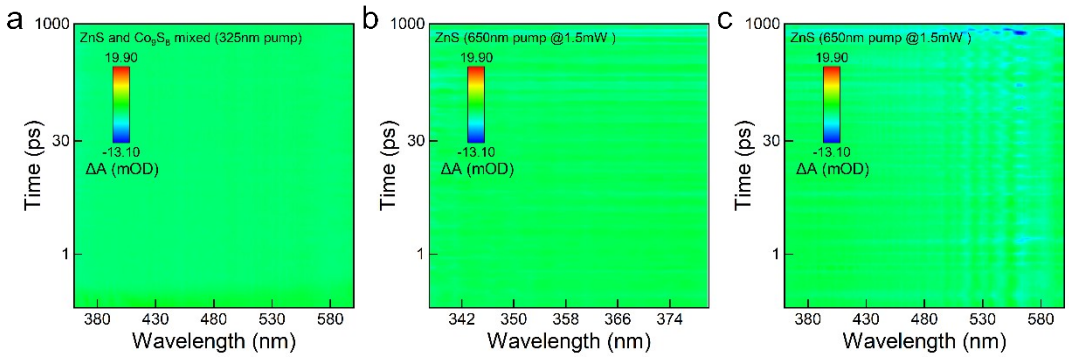

Fig. S9 Control experiments for the 509 nm GSB signal assignment. (a) fs-TA 2D pseudocolour map of a physical mixture of ZnS and Co_9S_8 nanoparticles under 325 nm pump@0.8 mW, probed in the UV-VIS region. (b) fs-TA 2D pseudocolour map of pristine ZnS under 650 nm pump@1.5 mW, probed in the UV region. (c) fs-TA 2D pseudocolour map of pristine ZnS under 650 nm pump@1.5 mW, probed in the VIS region.

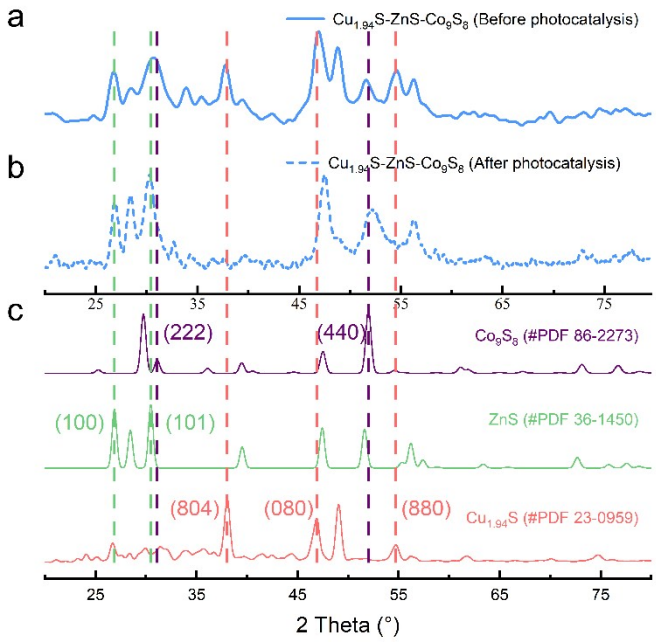

Fig. S10 XRD patterns of spherical CZC NHs before and after photocatalytic cycling. (a) XRD pattern of fresh CZC NHs. (b) XRD pattern of CZC NHs after four consecutive HER cycles over 24 h. (c) Simulated diffraction patterns of $Cu_{1.94}S$ (PDF#23-0959), ZnS (PDF#36-1450), and Co_9S_8 (PDF#86-2273)

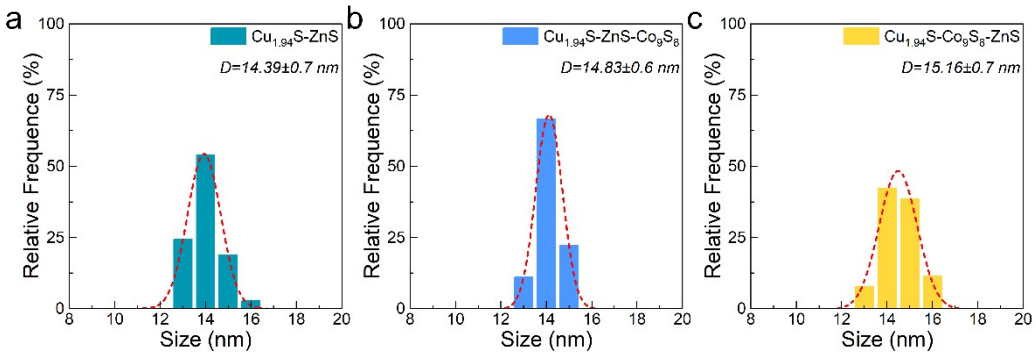

Fig. S11 TEM particle size distribution histograms. (a)CZ, (b)CZC and (c)CCZ. Particle diameters were measured from TEM images for each sample.

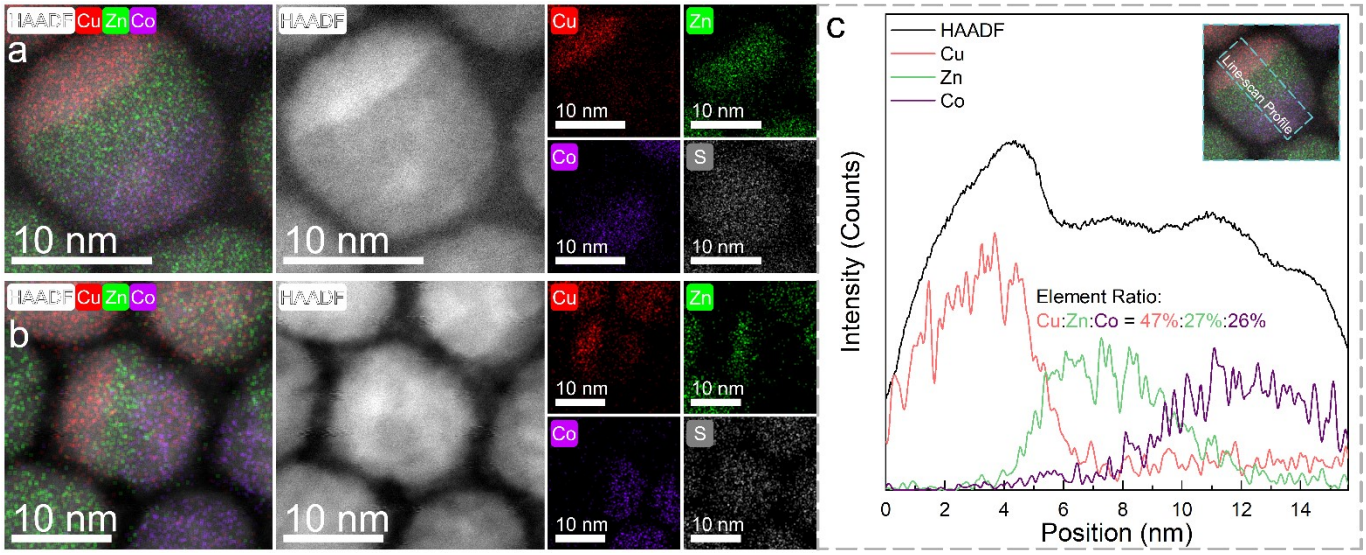

Fig. S12 STEM-EDS analysis of spherical CZC NHs. (a) HAADF-STEM image and the corresponding EDS elemental maps of Cu, Zn, Co, and S for a single CZC particle. (b) HAADF-STEM image and EDS elemental maps of a second CZC particle at a different magnification. (c) STEM-EDS line scan profile across the particle shown in (a).

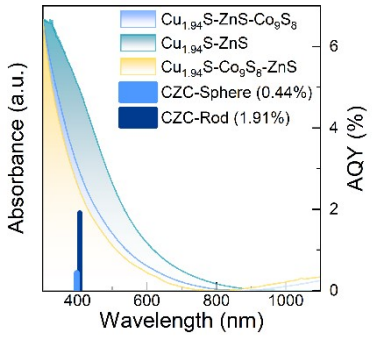

Fig. S13 UV-vis-NIR absorption spectra of spherical CZ, CZC and CCZ NHs and AQY values of spherical and rod-shaped CZC.

4. Experimental section

Synthesis of $Cu_{1.94}S$ Nanosphere: Spherical $Cu_{1.94}S$ nanocrystals were synthesized via a modified thermal decomposition method[1]. The reaction was conducted at 200℃ for 120 min, followed by immediate ice-water quenching to obtain a brown colloidal suspension. The product was flocculated with 40 mL ethanol, centrifuged at 8500 rpm for 10 min, and washed with hexane for 3 cycles via dispersion-centrifugation. The final products were stored as hexane colloids (10 mL) or vacuum-dried powders for subsequent use.

Preparation of precursor solution with Zn^{2+} and Co^{2+} for cation exchange: The precursor solution preparation followed a standardized protocol adapted from established cation exchange methodologies[2, 3]. Cobalt (II) and zinc chlorides were first oven-dehydrated (60°C, 24 hrs) to take out remaining moisture. For metal-ligand complex formation, precisely weighed anhydrous $CoCl_2$ or $ZnCl_2$ was combined with 24 mmol oleylamine (OLAm, ≈6.42 g) and 30 mmol 1-octadecene (ODE, ≈7.57 g) in a 250 mL three-neck flask equipped with reflux condenser, thermocouple, and argon inlet. The system underwent three vacuum-argon purge cycles via Schlenk line techniques at room temperature to establish an oxygen-free environment. Initial thermal activation involved vacuum heating to 80°C for 30 min to complete ligand dehydration. Under continuous argon run (100 $mL \cdot min^{-1}$), temperature was steadily raised to 200°C where the blend was continued for 30 min to form secure metal-OLAm coordination compound. The resulting precursor solutions were cooled under an inert atmosphere and stored in argon-purged containers with parafilm seals to prevent oxidation prior to cation exchange reactions.

The precursor solutions were prepared via a standardized cation exchange method. Anhydrous $CoCl_2$/$ZnCl_2$ (obtained by oven dehydration at 60 °C for 24 h) was mixed with 24 mmol OLAm and 30 mmol ODE in a three-neck flask. The system was subjected to three vacuum-argon purge cycles at room temperature, then heated to 80 °C under vacuum for 30 min for dehydration. The mixture was further heated to 200 °C under argon flow (100 $mL \cdot min^{-1}$) and held for 30 min to form stable metal-OLAm complexes. The precursor solutions were cooled and stored in argon-purged sealed containers before use.

Synthesis of binary $Cu_{1.94}S$-ZnS NHs: $Cu_{1.94}S$-ZnS NHs were synthesized via controlled cation exchange reaction. The Zn-OLAm complex was prepared as described above, and 60 mg of $Cu_{1.94}S$ nanospheres were dispersed in 4.36 g TOP via 10 min sonication under argon atmosphere. The colloidal suspension was rapidly injected into the Zn^{2+} precursor solution at 100 °C, and the reaction proceeded for 30 min. The product was quenched in an ice-water bath, and isolated via sequential centrifugation and precipitation cycles.

Synthesis of ZnS and Co_9S_8 NHs: ZnS and Co_9S_8 nanoparticles were synthesized via complete cation exchange reactions. For ZnS synthesis, a cation exchange solution containing 35 mmol ODE, 28.00 mmol OLAm and 1.40 mmol $ZnCl_2$ was degassed at 100 °C for 30 min under vacuum. 0.50 mmol $Cu_{1.94}S$ nanocrystals dispersed in 7.00 mmol ODE and 16.00 mmol TOP were injected into the preheated solution, and the exchange reaction was conducted at 100 °C for 30 min under Ar atmosphere.

Co_9S_8 nanoparticles were prepared via the same route with modified parameters: the exchange solution contained 30.00 mmol ODE, 24.00 mmol OLAm and 1.20 mmol $CoCl_2$; 0.50 mmol $Cu_{1.94}S$ nanocrystals were dispersed in 7.00 mmol ODE and 8.00 mmol TOP; the reaction was performed at 80 °C for 30 min under Ar flow. Both products were isolated via ethanol precipitation and stored under inert conditions.

Characterizations: The microstructure of the as-prepared nanocrystals was characterized by a field-emission scanning transmission electron microscope (FEI Titan G2 60-300 dual aberration-corrected S/TEM), with elemental distribution analysed via EDS. Phase identification was performed via X-ray diffraction (XRD) on a PANalytical Empyren system. Surface elemental composition and valence states were characterized by X-ray photoelectron spectroscopy (XPS, Thermo Scientific ESCALAB Xi, monochromatic Al Kα X-ray, 1486.6 eV). UV-vis-NIR absorption spectra were collected on a Shimadzu UV-1800 spectrophotometer in transmission mode. The as-prepared nanocrystals were thoroughly washed and re-dispersed in n-hexane to form a colloidal solution, and the measurement was performed using a quartz cuvette.

Hydrophilic surface modifications of NHs and NHs via ligand exchange: 10 mg of dehydrated photocatalyst was dispersed in 10 mL formic acid containing 3 vol% MPA at ambient temperature. The mixture was sonicated for 20 min to form a homogeneous dispersion, then magnetically stirred for 3 h to complete ligand anchoring. The functionalized photocatalyst was vacuum-dried at 25 °C for 12 h before subsequent tests.

Photoelectrochemical (PEC) measurements: PEC tests were performed in a standard three-electrode system, with a photocatalyst-coated FTO glass (1.0 cm × 1.0 cm) as the working electrode, platinum foil as the counter electrode, and Ag/AgCl (3 M KCl) as the reference electrode. The working electrode was prepared by spin-coating a photocatalyst colloidal suspension (1 $mg \cdot mL^{-1}$ in deionized water) on FTO substrate, followed by annealing at 300 °C under N_2 atmosphere. Electrochemical tests were conducted on a Metrohm Autolab PGSTAT302N workstation with a μStat-i 400 impedance module, in 0.1 M Na_2SO_4 electrolyte. Steady-state photocurrents were recorded at 0.4 V vs. Ag/AgCl under simulated solar irradiation (AM 1.5G, 100 mW/cm^2). Electrochemical impedance spectra (EIS) were collected in the frequency range of 10^5~10^{-1} Hz with 10 mV AC amplitude. Mott-Schottky analysis was performed at 10^3 Hz under dark conditions.

Table S1. XPS electron binding energies.

Sample	BE(eV)	Elements	Spectral Line
$Cu_{1.94}S$ NHs	161.5	S	$2p_{3/2}$
$Cu_{1.94}S$ NHs	162.6	S	$2p_{1/2}$
ZnS NHs	161.4	S	$2p_{3/2}$
ZnS NHs	162.7	S	$2p_{1/2}$
Co_9S_8 NHs	162.6	S	$2p_{3/2}$
Co_9S_8 NHs	163.9	S	$2p_{1/2}$
$Cu_{1.94}S$-ZnS NHs	161.1	S	$2p_{3/2}$
$Cu_{1.94}S$-ZnS NHs	162.3	S	$2p_{1/2}$
$Cu_{1.94}S$-Co_9S_8 NHs	161.9	S	$2p_{3/2}$
$Cu_{1.94}S$-Co_9S_8 NHs	163.2	S	$2p_{1/2}$
$Cu_{1.94}S$-ZnS-Co_9S_8 NHs	161.7	S	$2p_{3/2}$
$Cu_{1.94}S$-ZnS-Co_9S_8 NHs	163.0	S	$2p_{1/2}$
$Cu_{1.94}S$ -Co_9S_8-ZnS NHs	162.4	S	$2p_{3/2}$
$Cu_{1.94}S$ -Co_9S_8-ZnS NHs	163.5	S	$2p_{1/2}$
$Cu_{1.94}S$ NHs	932.4	Cu	$2p_{3/2}$
$Cu_{1.94}S$ NHs	952.3	Cu	$2p_{1/2}$
$Cu_{1.94}S$-ZnS NHs	932.1	Cu	$2p_{3/2}$
$Cu_{1.94}S$-ZnS NHs	951.9	Cu	$2p_{1/2}$
$Cu_{1.94}S$-Co_9S_8 NHs	932.3	Cu	$2p_{3/2}$
$Cu_{1.94}S$-Co_9S_8 NHs	952.1	Cu	$2p_{1/2}$
$Cu_{1.94}S$-ZnS-Co_9S_8 NHs	932.2	Cu	$2p_{3/2}$
$Cu_{1.94}S$-ZnS-Co_9S_8 NHs	952.1	Cu	$2p_{1/2}$
$Cu_{1.94}S$ -Co_9S_8-ZnS NHs	933.3	Cu	$2p_{3/2}$
$Cu_{1.94}S$ -Co_9S_8-ZnS NHs	953.0	Cu	$2p_{1/2}$
ZnS NHs	1021.6	Zn	$2p_{3/2}$
ZnS NHs	1044.7	Zn	$2p_{1/2}$
$Cu_{1.94}S$-ZnS NHs	1021.2	Zn	$2p_{3/2}$
$Cu_{1.94}S$-ZnS NHs	1044.3	Zn	$2p_{1/2}$
$Cu_{1.94}S$-ZnS-Co_9S_8 NHs	1022.0	Zn	$2p_{3/2}$
$Cu_{1.94}S$-ZnS-Co_9S_8 NHs	1045.0	Zn	$2p_{1/2}$
$Cu_{1.94}S$ -Co_9S_8-ZnS NHs	1022.8	Zn	$2p_{3/2}$
$Cu_{1.94}S$ -Co_9S_8-ZnS NHs	1045.8	Zn	$2p_{1/2}$

Sample	BE(eV)	Elements	Spectral Line
Co_9S_8 NHs	778.5	Co^{3+}	$2p_{3/2}$
Co_9S_8 NHs	793.6	Co^{3+}	$2p_{1/2}$
Co_9S_8 NHs	781.1	Co^{2+}	$2p_{3/2}$
Co_9S_8 NHs	797.2	Co^{2+}	$2p_{1/2}$
Co_9S_8 NHs	785.6	Co Satellite	$2p_{3/2}$
Co_9S_8 NHs	802.7	Co Satellite	$2p_{1/2}$
$Cu_{1.94}S$-Co_9S_8 NHs	778.5	Co^{3+}	$2p_{3/2}$
$Cu_{1.94}S$-Co_9S_8 NHs	793.5	Co^{3+}	$2p_{1/2}$
$Cu_{1.94}S$-Co_9S_8 NHs	781.2	Co^{2+}	$2p_{3/2}$
$Cu_{1.94}S$-Co_9S_8 NHs	797.0	Co^{2+}	$2p_{1/2}$
$Cu_{1.94}S$-Co_9S_8 NHs	785.9	Co Satellite	$2p_{3/2}$
$Cu_{1.94}S$-Co_9S_8 NHs	803.0	Co Satellite	$2p_{1/2}$
$Cu_{1.94}S$-ZnS-Co_9S_8 NHs	778.5	Co^{3+}	$2p_{3/2}$
$Cu_{1.94}S$-ZnS-Co_9S_8 NHs	793.1	Co^{3+}	$2p_{1/2}$
$Cu_{1.94}S$-ZnS-Co_9S_8 NHs	781.3	Co^{2+}	$2p_{3/2}$
$Cu_{1.94}S$-ZnS-Co_9S_8 NHs	797.2	Co^{2+}	$2p_{1/2}$
$Cu_{1.94}S$-ZnS-Co_9S_8 NHs	786.4	Co Satellite	$2p_{3/2}$
$Cu_{1.94}S$-ZnS-Co_9S_8 NHs	802.5	Co Satellite	$2p_{1/2}$
$Cu_{1.94}S$ -Co_9S_8-ZnS NHs	779.4	Co^{3+}	$2p_{3/2}$
$Cu_{1.94}S$ -Co_9S_8-ZnS NHs	797.2	Co^{3+}	$2p_{1/2}$
$Cu_{1.94}S$ -Co_9S_8-ZnS NHs	782.2	Co^{2+}	$2p_{3/2}$
$Cu_{1.94}S$ -Co_9S_8-ZnS NHs	798.5	Co^{2+}	$2p_{1/2}$
$Cu_{1.94}S$ -Co_9S_8-ZnS NHs	786.7	Co Satellite	$2p_{3/2}$
$Cu_{1.94}S$ -Co_9S_8-ZnS NHs	803.4	Co Satellite	$2p_{1/2}$

Table S2. Femtosecond transient absorption spectra of kinetic profiles

325 nm pump

Sample	Wavelength (nm)	Signal Type	τ_1 (ps)	τ_2 (ps)	τ_3 (ps)
$Cu_{1.94}S$	369	GSB	47.37	973.2	—
	445	ESA	70.35	1006	—
	509	ESA	54.21	934.2	—
	580	ESA	2.895	545.6	—
	817	ESA	0.759	174.5	—
	866	ESA	0.557	182.6	—
ZnS	369	—	0.096	53.61	—
	445	—	0.378	58.42	—
	509	—	3.938	101.6	—
	580	—	5.03	177.4	—
	817	—	0.759	174.5	—
	866	—	0.557	182.6	—
Co_9S_8	369	—	0.215	48.25	—
	445	—	37.26	662.8	—
	509	—	1.422	68.43	—
	580	—	43.92	312.5	—
$Cu_{1.94}S$-ZnS	369	—	21.57	567.5	—
	445	—	76.15	686.9	—
	509	ESA	55.56	716.4	—
	580	ESA	10.59	619.7	—
	817	ESA	1.227	599	—
	866	ESA	1.373	495.3	—
$Cu_{1.94}S$-ZnS-Co_9S_8	369	ESA	13.84	195.9	—
	445	ESA	12.57	143.3	—
	509	GSB	1.55	12.4	46.49
	580	ESA	5.136	59.81	—
	817	ESA	1.689	34.41	—
	866	ESA	1.818	13.45	43.18
$Cu_{1.94}S$-Co_9S_8-ZnS	369	ESA	0.258	21.99	—
	445	ESA	17.33	82.69	—
	509	GSB	0.523	14.56	125.7
	580	ESA	5.524	51.82	—
	817	ESA	1.647	32	—
	866	ESA	0.89	14.24	158.5

650 nm pump

Sample	Wavelength (nm)	Signal Type	τ_1 (ps)	τ_2 (ps)	τ_3 (ps)
$Cu_{1.94}S$	369	ESA	164.7	—	—
	445	ESA	41.3	1314	—
	415	ESA	8.261	1111	—
	509	—	76.12	1334	—
$Cu_{1.94}SZnS$	369	—	0.362	846.9	—
	445	—	130	1622	—
	509	—	7.641	630.9	—
	550	ESA	0.078	472.8	—
$Cu_{1.94}S$-ZnS-Co_9S_8	369	ESA	3.205	32.22	—
	445	ESA	0.099	37.42	—
	509	GSB	0.43	22.66	67.8
	580	ESA	0.192	33.76	—
$Cu_{1.94}S$-Co_9S_8-ZnS	369	ESA	2.911	30.73	—
	445	ESA	0.922	40.31	—
	509	GSB	0.916	31.54	131.5
	580	ESA	2.94	39.38	—

Table S3. Information of Chemicals used in synthesis and experiments.

Chemicals	CAS No.	Purity	Formula	Manufacturer	Cat. No.
Copper acetylacetonate	13395-16-9	≥97%	$Cu(acac)_2$	Aladdin Scientific Corp.	C109323
Zinc chloride	7646-85-7	≥98%	$ZnCl_2$	Aladdin Scientific Corp.	Z112526
Cobalt (II) chloride	7646-79-9	99.7%	$CoCl_2$	Aladdin Scientific Corp.	C106772
1-Octadecene	112-88-9	>90%	$C_{18}H_{36}$	Aladdin Scientific Corp.	O109487
Oleylamine	112-90-3	80-90%	$C_{18}H_{37}N$	Aladdin Scientific Corp.	O106967
Trioctylphosphine	4731-53-7	90%	$C_{24}H_{51}P$	Aladdin Scientific Corp.	T106625
Tert-dodecanethiol	25103-58-6	98%	$C_{12}H_{26}S$	Aladdin Scientific Corp.	D106952
3-Mercaptopropionic acid	107-96-0	98%	$C_3H_6O_2S$	Aladdin Scientific Corp.	M103035
Formamide	75-12-7	99%	CH_3NO	Aladdin Scientific Corp.	F103361
Sodium sulfite	7757-83-7	98%	Na_2SO_3	Aladdin Scientific Corp.	S112300
Sodium sulfide nonahydrate	1313-84-4	≥98%	$Na_2S{\cdot}9H_2O$	Aladdin Scientific Corp.	S299093
Absolute ethanol	64-17-5	≥99.8%	CH_3CH_2OH	Sinopharm Chemical Reagent Co. Ltd.	10009259
Hexane	110-54-3	≥97.0%	$CH_3(CH_2)_4CH_3$	Sinopharm Chemical Reagent Co. Ltd.	800686191

Table S4. Summary for different systems for hydrogen production.

Photocatalyst	**HER efficiency (μmol h^{-1} g^{-1})**	**toxic metal**	**noble metal**	**Ref**
$Cu_{1.94}S$-ZnS-Co_9S_8	1047	no	no	This work
$CaTiO_3$/CdS	12,381.8	yes	no	[4]
TiO_2–NiS_x	981.59	no	no	[5]
Cu@TiO_2-Cu_2O	12,000.6	no	no	[6]
$Ni(OH)_2$-TiO_2-Cu_2O	8,384.84	no	no	[7]
Pt/CdS-D	6,295	yes	yes	[8]
$ZnIn_2S_4$/$LaNiO_3$	1,600	no	no	[9]
$CoMoO_4$/Carbon Nitride	8,350	no	no	[10]
CuO/Carbon Nitride	10,400	no	no	[11]
CdS/Co_9S_8	1,061	yes	no	[12]
CdS QDs@Co_9S_8	9642.7	yes	no	[13]
Co_9S_8/RP	1,562.5	no	no	[14]
Co_9S_8/$Zn_{0.5}Cd_{0.5}S$	10,156	yes	no	[15]
Co_9S_8/$ZnIn_2S_4$	12,670	no	no	[16]

Table S5. Tri-exponential fitting parameters for the 509 nm GSB kinetics of CZC and CCZ under 325 nm and 650 nm excitation.

325 nm pump

Sample	Wavelength (nm)	τ_1 (ps)	A_1	τ_2 (ps)	A_2	τ_3 (ps)	A_3	Standard deviation
$Cu_{1.94}S$-ZnS-Co_9S_8	509	1.55	-0.05996	12.4	-0.07158	46.49	-0.05615	0.00850
$Cu_{1.94}S$-Co_9S_8-ZnS	509	0.523	-0.04283	14.56	-0.03314	125.7	-0.01856	0.00329

650 nm pump

Sample	Wavelength (nm)	τ_1 (ps)	A_1	τ_2 (ps)	A_2	τ_3 (ps)	A_3	Standard deviation
$Cu_{1.94}S$-ZnS-Co_9S_8	509	0.43	-0.03220	22.66	-0.03634	67.8	-0.03363	0.00433
$Cu_{1.94}S$-Co_9S_8-ZnS	509	0.916	-0.01235	31.54	-0.02531	131.5	-0.01165	0.00105

Table S6. Metal ratios of spherical CZC NHs determined by EDS before photocatalysis and by ICP-OES after four consecutive HER cycles over 24 h.

Element ratio / Photocatalyst	Cu (%)	Zn (%)	Co (%)
CZC Before photocatalysis (line-scan)	47	27	26
CZC After photocatalysis (ICP-OES)	36	37	27

Reference

1. X. Y. Guo, S. Liu, W. J. Wang, et al., *J. Colloid Interface Sci.*, 2021, **600**, 838-846.
2. B. C. Steimle, J. L. Fenton and R. E. Schaak, *Science*, 2020, **367**, 418-424.
3. C. R. McCormick, S. M. Baksa, J. M. Veglak, et al., *Chem. Mater.*, 2023, **35**, 5433-5446.
4. W. Zhang, J. Xiong, S. Li, et al., *Molecular Catalysis*, 2025, **570**, 114701.
5. Y. Wei, G. Cheng, J. Xiong, et al., *Journal of Energy Chemistry*, 2019, **32**, 45-56.
6. P. Qiu, J. Xiong, M. Lu, et al., *J Colloid Interface Sci*, 2022, **622**, 924-937.
7. C. Wang, J. Xiong, Z. Wen, et al., *Industrial & Engineering Chemistry Research*, 2023, **62**, 11402-11413.
8. J. Deng, X. Xu, B. Su, et al., *Materials Horizons*, 2025, **12**, 5702-5709.
9. Z. Wang, B. Su, J. Xu, et al., *Int. J. Hydrog. Energy*, 2020, **45**, 4113-4121.
10. J. Qin, Y. Dong, X. Lai, et al., *J. Mater. Sci. Technol.*, 2024, **198**, 176-185.
11. J. Qin, Y. Zhang, M. Duan, et al., *Int. J. Hydrog. Energy*, 2025, **188**.
12. B. Qiu, Q. Zhu, M. Du, et al., *Angew Chem Int Ed Engl*, 2017, **56**, 2684-2688.
13. Y. Yan, Y. Wu, C. Lu, et al., *Molecules*, 2024, **29**.
14. F. Zhao, M. Zhang, D. Yan, et al., *ACS Applied Nano Materials*, 2023, **6**, 14478-14487.
15. Q. Xu, L. Liu, H. T. Xia, et al., *Colloids Surf., A*, 2023, **667**, 131404.
16. Q. C. Li, Q. F. Lu, E. Y. Guo, et al., *Energy & Fuels*, 2022, **36**, 4541-4548.